



Investigation of photoluminescence and dielectric properties of europium-doped LaOCl nanophosphor and its Judd–Ofelt analysis

S. R. Yashodha^{1,2}, N. Dhananjaya^{2,*} , S. R. Manohara³, and H. S. Yogananda⁴

¹Department of Physics, Don Bosco Institute of Technology (Affiliated to Visveswaraya Technological University - Belagavi), Bangalore, Karnataka 560 074, India

²Centre for Advanced Materials Research Lab, Department of Physics, BMS Institute of Technology and Management (Affiliated to Visveswaraya Technological University - Belagavi), Bangalore, Karnataka 560 064, India

³Nano-Composites and Materials Research Lab, Department of Physics, Siddaganga Institute of Technology (Affiliated to Visveswaraya Technological University - Belagavi), Tumakuru, Karnataka 572 103, India

⁴Department of Physics, Sai Vidya Institute of Technology (Affiliated to Visveswaraya Technological University - Belagavi), Bangalore, Karnataka 560 064, India

Received: 17 September 2020

Accepted: 8 March 2021

Published online:

15 April 2021

© The Author(s), under exclusive licence to Springer Science+Business Media, LLC, part of Springer Nature 2021

ABSTRACT

Present Phosphor $\text{La}_{1-x}\text{Eu}_x\text{OCl}$ ($0 \leq x \leq 0.09$) was synthesized via conventional solid-state method at a temperature of 700 °C for a duration of 2 h. The compound crystallized in the tetragonal structure with space group $P4/nmm$ (No. 129). The intensity of transition ${}^5\text{D}_0 \rightarrow {}^7\text{F}_2$ (617 nm) was found to be more intense in the photoluminescence spectra. Intensity parameters and radiative properties like radiative lifetime, transition probabilities, and branching ratio are evaluated employing of the Judd–Ofelt theory. At room temperature for a frequency range of 10 Hz–8 MHz, AC conductivity, dielectric properties of $\text{La}_{1-x}\text{Eu}_x\text{OCl}$ ($0.01 \leq x \leq 0.09$) are studied. Studies indicate that above 30 kHz till 100 kHz, the AC conductivity establishes slowly and at 300 kHz increases rapidly. Greater values of dielectric constant and loss were exhibited towards lower frequencies which then declined significantly with increasing frequency making the phosphor suitable for microwave device applications. The CIE color coordinates results of Eu^{3+} -activated LaOCl phosphor (0.642, 0.358) were closer to the commercial red phosphors such as $\text{Y}_2\text{O}_3:\text{Eu}^{3+}$ (0.645, 0.347), $\text{Y}_2\text{O}_2\text{S}:\text{Eu}^{3+}$ (0.647, 0.343) and National Television System Committee (NTSC) (0.67, 0.33) resulting in making $\text{LaOCl}:\text{Eu}^{3+}$ behaves as a promising material for red phosphor materials.

Address correspondence to E-mail: ndhananjayas@bmsit.in

Table 1 Calculated crystallite size from PXRD peak broadening for $\text{La}_{1-x}\text{Eu}_x\text{OCl}$

Concentration of Eu^{3+}	0.00	0.01	0.03	0.05	0.07	0.09
Scherrer's method (nm)	37.44	38.59	36.75	35.71	37.88	37.20
W-H method (nm)	32.02	31.6	31.89	31.5	32.06	31.75

1 Introduction

RE^{3+} -activated oxyhalides phosphor of lanthanides is utilized in broad areas of applications in the industry [1]. Lanthanum oxyhalides (LaOX , $X = \text{Cl}, \text{Br}, \text{F}$) enclose distinctive, exceptional optical, magnetic, electrical, and luminescent behavior [2, 3]. Due to their ability as phosphor hosts, luminescence properties of these materials are examined broadly [4, 5]. The RE^{3+} are generally included in materials as trivalent cation to comprehend optically active substances in optoelectronic, photonic applications. In phosphors for many reasons, europium serves to be an efficient luminescent center [6, 7]. To observe color red on displays of a variety of electronic devices, phosphors with europium as dopant ions are significant. In nanocrystalline form these materials has numerous potential uses in the field of chemical/biological sensors, light emitting devices, photocatalysis, and solar energy conversion [8–10].

Intensity parameters and radiative properties like branching ratio, radiative lifetime, and transition probabilities are basic property that characterizes optical materials for their utility in laser devices and photonics [11]. Using the theory of Judd–Ofelt analysis, all the above quantities may be estimated from either the absorption or emission spectrum of the phosphor. Two physicists Judd [12] and Ofelt [13], discretely found an electronic model to evaluate the spectral parameter of ions of rare earth. In-depth, the knowledge of the function of these parameters is required to devise phosphor with enviable luminescence. Commonly the spectral intensities with their relative ratios characterize the rare-earth ions. Judd–Ofelt (JO) theory helps in explaining the nature of rare-earth dopants rooted inside the host. According to this theory, mixed parity states are produced due to crystal field effects and could be known through JO parameters which are reactive to the local environment [12, 13]. It is important to study the variation of AC electrical conductivity with the frequency of the applied electric field, as most of the electrical appliances rely on electrical modes of operations [15].

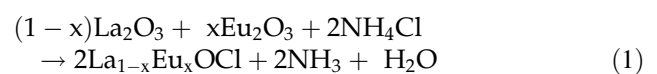
Synthesis of LaOCl can be done via various methods, including liquid-phase method [16], solid-state [17], combustion [18], sol–gel [19], solvothermal and surfactant-assisted solvothermal reaction [20], mechanochemical grinding [21]. Of all these methodologies, solid-state reaction proposes numerous merits like large scale production, high purity of products, solvent/surfactant-free process, and enhanced control over composition.

The present paper reports the preparation of $\text{La}_{1-x}\text{Eu}_x\text{OCl}$ ($x = 0.0$ to 0.09) phosphors via solid-state route in a short time at comparatively low temperature. The crystallographic structural parameters, functional groups are determined by PXRD, FTIR spectroscopy, respectively. Energy bandgap and morphological studies are done using UV–Visible spectra and SEM/TEM analysis. The photoluminescence and CIE analysis of the sample are carried out. Besides, the Judd–Ofelt intensity parameters, radiative emission rates, branching, lifetime, and asymmetry ratios are evaluated with the emission spectra. At room temperature, the AC conductivity, $\tan \delta$, and dielectric constant are examined as a function of frequency.

2 Experimental

2.1 Synthesis

A conventional solid-state route was adopted for the synthesis of Eu^{3+} -activated LaOCl phosphor. Rare-earth oxides La_2O_3 , Eu_2O_3 , and NH_4Cl are the initial materials. Calcination of all rare-earth oxides at 800°C for 6 h is done before weighing. Using pestle in an agate mortar, the stoichiometric amount of La_2O_3 , Eu_2O_3 , and NH_4Cl (excess 20%) were ground thoroughly. The mixed powder was taken in porcelain crucible, calcined at 700°C for 2 h (ambient atmosphere) which is bought down to room temperature.



2.2 Characterizations

PANalyticalX'Pert Pro powder diffractometer with nickel filter using Cu K α radiation ($\lambda = 0.15418$ nm) was utilized to examine the phase purity of the compounds. SEM analysis was done using ESEM quanta 200, FEI. HRTEM was examined using Jeol/JEM 2100 with 0.23 nm point resolution and 0.14 nm lattice resolution. Using KBr as a reference, FTIR and UV–Visible absorption spectra are noted from Perkin Elmer spectrometer Frontier and Perkin Elmer Lambda 750 spectrophotometer, respectively. JobinYvon spectrofluorometer (Fluorolog-3, Horiba) fortified with a 450 W xenon lamp as an excitation source was used to carry out the PL studies. With Hioki IM3536 LCR meter from a frequency of 10 Hz to 8 MHz, AC conductivity and dielectric property of phosphor are studied. Under room temperature, all the measurements were made.

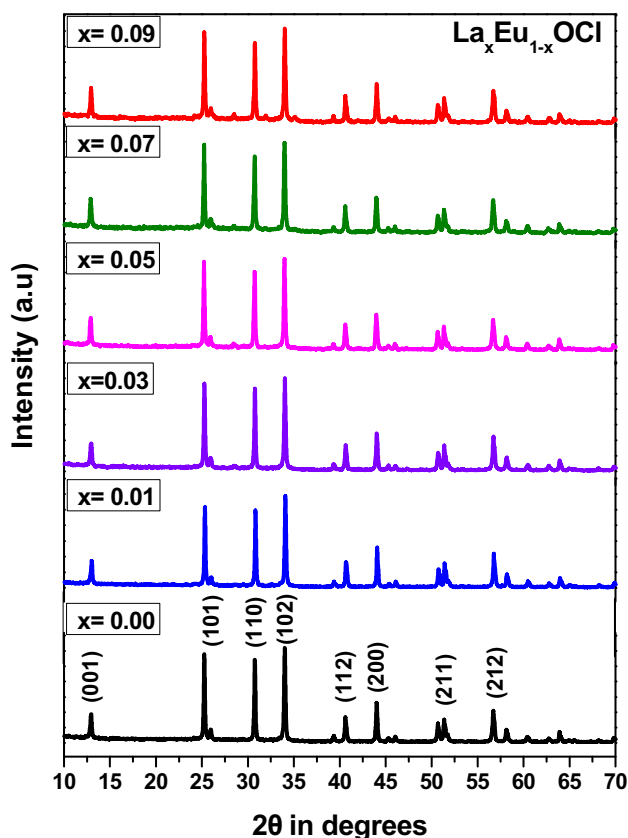


Fig. 1 PXR D patterns of $\text{La}_{1-x}\text{Eu}_x\text{OCl}$ ($0.00 \leq x \leq 0.09$) nanophosphors

3 Results and discussion

3.1 Powder X-ray diffraction

Figure 1 represents X-ray diffractogram of $\text{La}_{1-x}\text{Eu}_x\text{OCl}$ ($0 \leq x \leq 0.09$) compound. A single-phase Eu^{3+} -doped LaOCl compound is confirmed from the sharp and single diffraction peaks of the XRD spectrum. No obvious shifting of peaks or other impurity phases can be detected in the Eu^{3+} -doped samples, indicating that the Eu^{3+} ions are efficiently incorporated in the LaOCl host lattice by replacing the La^{3+} [35]. With the space group $P4/nmm$, a tetragonal (PbFCl-type) structure has been exhibited by the phosphor [18, 19]. $a = 0.4121$ nm, $b = 0.4121$ nm, $c = 0.6884$ nm were the unit cell lattice parameters with $\alpha = \beta = \gamma = 90^\circ$. In LaOCl , Eu^{3+} can get substituted into the cationic site available; to validate this acceptable percentage ionic radius (D_r) may be evaluated. Between the dopant and substituted cation, the percentage ionic difference (D_r) shall not go above $\sim 15\%$ for the substitution of dopant [14]. The following formula is used to calculate the difference in ionic radii:

$$D_r = \frac{R_h(\text{CN}) - R_d(\text{CN})}{R_h(\text{CN})} \quad (2)$$

here R_h (CN) and R_d (CN) represents radius of host cation and doped ion respectively. Upon substitution of the ionic radii of Eu^{3+} and La^{3+} respectively, the D_r between them is obtained to be 8.24%. Thus Eu^{3+} evidently would replace the Lanthanum site in LaOCl .

The grain size measurements are done by means of Debye–Scherrer formula:

$$d = \frac{k\lambda}{\beta \cos\theta} \quad (3)$$

here, $k = 0.9 =$ constant, $d =$ grain size, $\beta =$ full-width at half maximum (FWHM), $\lambda =$ wavelength of the X-ray radiation and $\theta =$ angle of diffraction. The determined grain size of Eu^{3+} doped LaOCl lies between 35–37 nm.

The particle size also was found using FWHMs of the diffraction peaks. The FWHMs (β) could be written as a linear combination of influences from the particle size (d) and strain (ϵ) using the Hall and Williamson relation [22]:

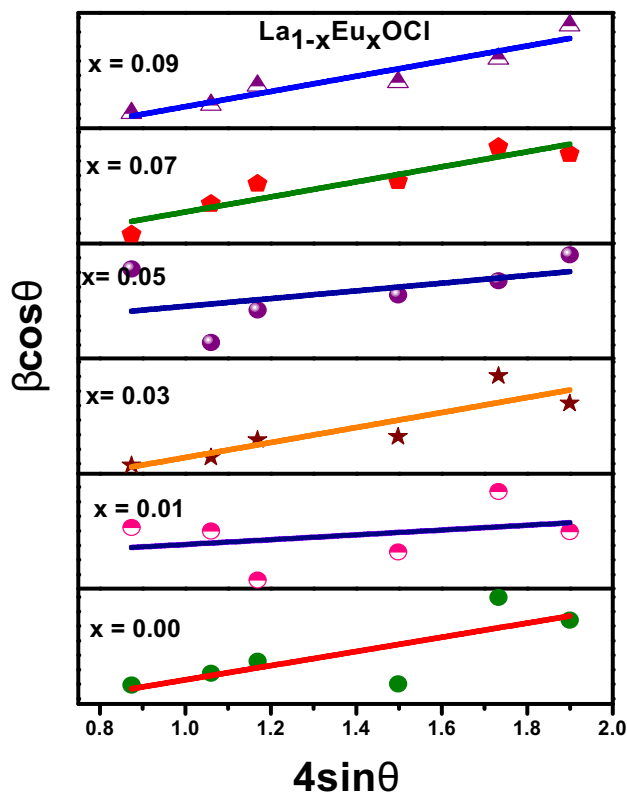


Fig. 2 W–H plots of $\text{La}_{1-x}\text{Eu}_x\text{OCl}$ ($0.00 \leq x \leq 0.09$) nanophosphors

$$\beta \cos \theta = \frac{0.9\lambda}{d} + 4\epsilon \sin \theta \quad (4)$$

A straight-line graph is obtained by plotting $\beta \cos \theta / \lambda$ vs $\sin \theta / \lambda$ for Eu^{3+} doped LaOCl Fig. 2. On the $\beta \cos \theta / \lambda$ axis, the reciprocal of intercept particle as 32 nm which provides the mean size of is in accord with the evaluated value by Debye–Scherrer formula.

3.2 SEM and TEM analysis

Figure 3a and b represent SEM micrographs and the composition of elements of $\text{La}_{1-x}\text{Eu}_x\text{OCl}$ ($x = 0.07$) phosphor. An agglomeration is exhibited by the nanophosphor which can be attributed to the method of synthesis.

TEM and HRTEM of $\text{La}_{1-x}\text{Eu}_x\text{OCl}$ ($x = 0.07$) phosphor help in the understanding of particle size distribution. Closer examination of TEM images in Fig. 4a reveal that the phosphor is in the nano regime. The lattice fringes as seen in Fig. 4b with 0.34 nm as the interplanar distance that matches the plane (101) in LaOCl . Diffraction circles composed of diffraction dot is exhibited in Fig. 4c SAED pattern of $\text{La}_{1-x}\text{Eu}_x\text{OCl}$ ($x = 0.07$).

3.3 FTIR spectra

Figure 5 represents the Fourier transform spectra of $\text{La}_{1-x}\text{Eu}_x\text{OCl}$ ($0.00 \geq x \geq 0.09$) nanophosphor in the range $450\text{--}4000\text{ cm}^{-1}$. In the lower frequency domain at 510 cm^{-1} (La–O) vibration peaks of metal–oxygen bands appeared [23]. The band at 1594 cm^{-1} represents asymmetric stretching vibrations of C = O carboxyl groups, while bands at 1383 and 3461 cm^{-1} correspond to the bending and stretching bands of the O–H group correspondingly [22].

3.4 Energy bandgap analysis

Figure 6 shows the bandgap energy for $\text{La}_{1-x}\text{Eu}_x\text{OCl}$ ($0 \leq x \leq 0.09$). The energy bandgap is determined using Wood and Tauc relation from the data of absorption Spectra:

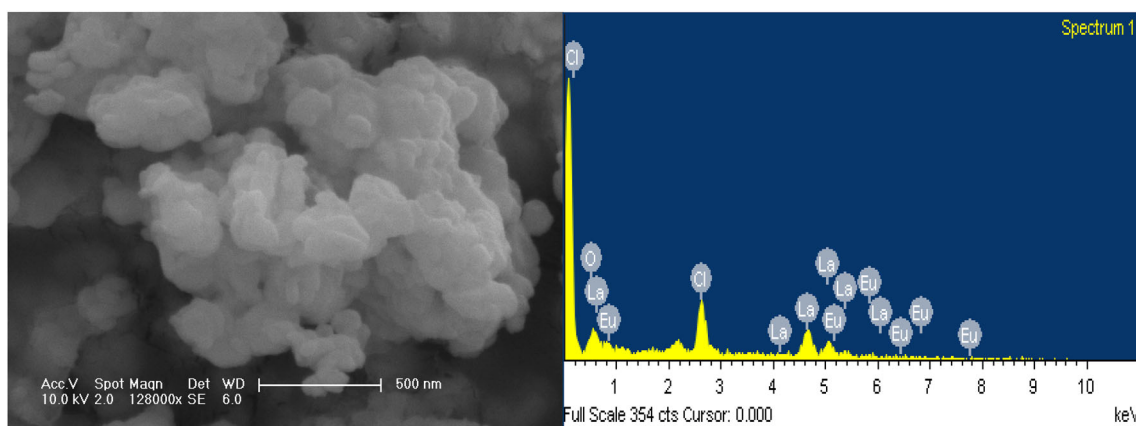


Fig. 3 a FE-SEM micrographs and b EDAX spectrum of $\text{La}_{0.93}\text{Eu}_{0.07}\text{OCl}$ nanophosphors

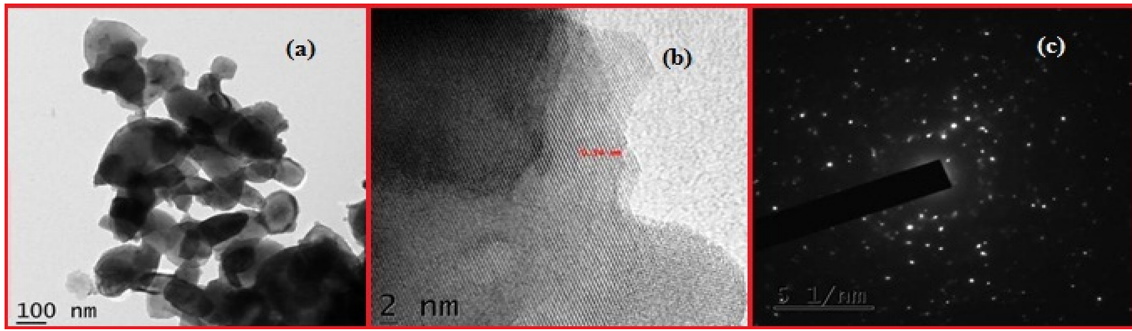


Fig. 4 **a** TEM image. **b** HR-TEM. **c** SAED of $\text{La}_{0.93}\text{Eu}_{0.07}\text{OCl}$ nanophosphors

$$\alpha h\nu = A(h\nu - E_g)^n \tag{5}$$

$h\nu$ is photon energy, α denotes co-efficient of absorption, A = constant of proportionality, E_g = energy bandgap, and n relies on properties of transition in a semiconductor. $n = 1/2, 2, 3/2$ or 3 for allowed direct, allowed indirect, forbidden direct, forbidden indirect electronic transitions, respectively. For LaOCl nanophosphor the absorption spectrum is governed through direct electronic transition, n is $1/2$ [24]. The intercept of the tangent to x - axis provides the value of energy gap and is found to be in the

range of 4.165–4.22 eV for $\text{La}_{1-x}\text{Eu}_x\text{OCl}$ ($0 \leq x \leq 0.09$) nanophosphors.

3.5 Photoluminescence

Figure 7a and b represent excitation and emission spectra of $\text{La}_{1-x}\text{Eu}_x\text{OCl}$ nanophosphors, respectively. The luminescence of Eu^{3+} ions attributes to the phenomenon of excitation which is due to $\text{Eu}^{3+} - \text{O}^{2-}$ charge transfer (CT), enhancing the emission effectiveness along with sensitizing phosphors for series of short-wave UV (254 nm) [25]. The 395 nm (${}^7\text{F}_0 \rightarrow {}^5\text{L}_6$) excitation wavelength corresponds to $4f-4f$ transitions of Eu^{3+} ions in the host lattice. On excitation at 395 nm, a set of emission lines were exhibited by the spectra that relates the transitions from ${}^5\text{D}_0$ level of excitation to ground levels ${}^7\text{F}_j$ ($j = 1, 2, 3, 4$) of the $\text{Eu}^{3+}4f_6$ configuration. The transition ${}^5\text{D}_0 \rightarrow {}^7\text{F}_0$ owes to J-mixing by the crystal field effects. ${}^5\text{D}_0 \rightarrow {}^7\text{F}_1$ and ${}^5\text{D}_0 \rightarrow {}^7\text{F}_2$ transitions were of specific importance among all as they signify the local environment of Eu^{3+} ion. The ${}^5\text{D}_0 \rightarrow {}^7\text{F}_1$ transition peaks originate from the magnetic dipole transition. On the contrary, the radiative transitions from ${}^5\text{D}_0$ to ${}^7\text{F}_2$ and ${}^7\text{F}_4$ levels are induced by an electric dipole in nature. The ${}^5\text{D}_0 \rightarrow {}^7\text{F}_3$ (650 nm) transition is prohibited from both magnetic and electric dipole considerations. Magnetic dipole (${}^5\text{D}_0 \rightarrow {}^7\text{F}_1$) emission transition was predominant, as the Eu^{3+} ion was located at the site with inversion symmetry, further induced electric dipole (${}^5\text{D}_0 \rightarrow {}^7\text{F}_2$) transition becomes dominant at a site without inversion symmetry [14]. For $\text{La}_{1-x}\text{Eu}_x\text{OCl}$ phosphors, Eu^{3+} ions essentially occupy site without inversion symmetry in LaOCl host lattice as the intensity of emission for ${}^5\text{D}_0 \rightarrow {}^7\text{F}_2$ (617 nm) was stronger than ${}^5\text{D}_0 \rightarrow {}^7\text{F}_1$ (595 nm). Splitting in ${}^5\text{D}_0 - {}^7\text{F}_2$ transition can be due to the stark effect (splitting

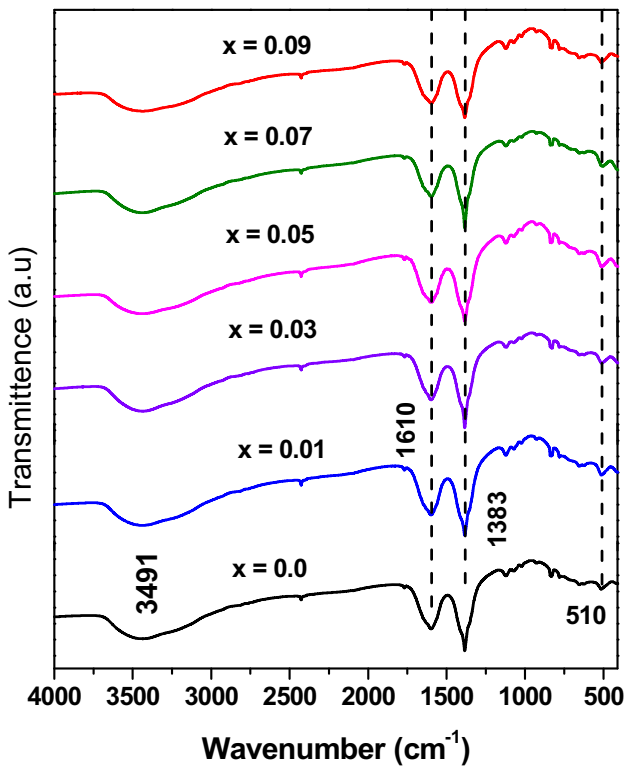


Fig. 5 FTIR spectra of $\text{La}_{1-x}\text{Eu}_x\text{OCl}$ ($0.00 \leq x \leq 0.09$) nanophosphors

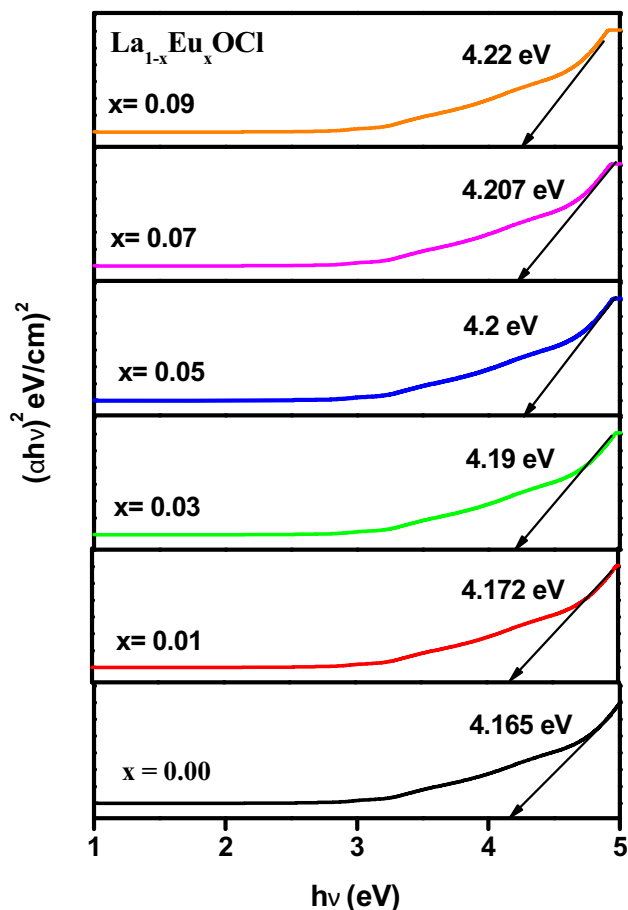


Fig. 6 Energy bandgap diagram of $\text{La}_{1-x}\text{Eu}_x\text{OCl}$ ($0.00 \leq x \leq 0.09$) nanophosphors

of energy levels due to the external electric field or crystal field). Crystal field splits the excited energy levels of rare-earth ions into a number of sublevels thereby increasing the probability of transition near the expected wavelength inducing more peaks in the spectrum. By increasing the Eu^{3+} doping concentration (1–9 mol %), the relative intensity of $^5\text{D}_0 \rightarrow ^7\text{F}_2$ transition (617 nm) increases up to 7 mol% and thereafter decreases due to quenching. Quenching effect appears because of the non-radiative energy transfer owing to radiation re-absorption, exchange interaction, or multipole-multipole interaction.

To begin with, the transfer of energy occurs due to the rate of re-absorption of radiation as an impact of a broad overlap of fluorescent spectra of the activator and sensitizer [26]. Clearly from the PL spectra, it is seen that the quenching effect is not due to radiation re-absorption.

Next, according to Blasse et al., R_c the critical transfer distance is written as [27]

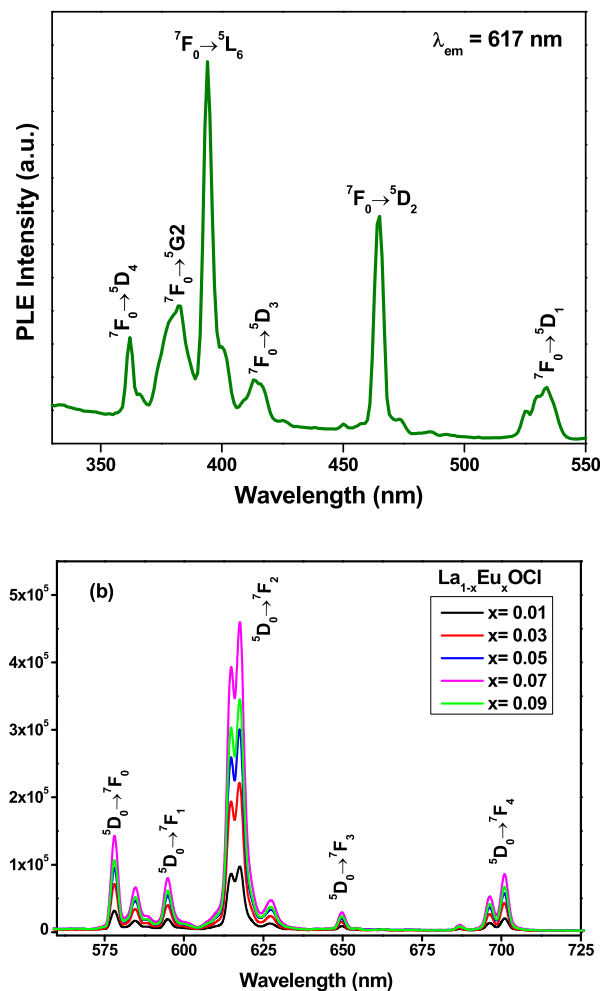


Fig. 7 **a** Excitation spectra and **b** Emission spectra of $\text{La}_{1-x}\text{Eu}_x\text{OCl}$ ($0.01 \leq x \leq 0.09$) nanophosphors

$$R_c = 2 \left[\frac{3V}{4X_c\pi N} \right]^{1/3} \quad (6)$$

$V = 0.117 \text{ (nm)}^3 = a^2c$ is unit cell volume, $X_c = 0.07$ is concentration of Eu^{3+} ion (optimum), $N = 4$ in a unit cell the no. of vacant cationic sites for LaOCl . The non-radiative transfer of energy occurs only if R_c value is less than 3–4 Å [28]. For $\text{La}_{1-x}\text{Eu}_x\text{OCl}$, 9.28 Å is obtained as its critical transfer distance R_c inferring the transfer of energy is not because of exchange interaction for LaOCl .

Lastly, if the energy transfer is relative to $(x)^{\theta/3}$ where $x = C / C^*$ = concentration of dopant, C is quenching ion concentration, and C^* is critical transfer concentration of quenching then the multipolar interaction tends to non-radiative energy transfer. $\theta = 6, 8$ or 10 indicates dipole-dipole, dipole-quadruple or quadruple-quadruple

interaction correspondingly [29]. Transfer of energy in the host matrix is given by correlation of emission intensity and activator and can be written as:

$$\frac{I}{x} = k [1 + \beta x^{\theta/3}]^{-1} \tag{7}$$

k and β = constants, $\frac{I}{x}$ = emission intensity per activator ion. Relation (7) may also be written as:

$$\log\left(\frac{I}{x}\right) = k' - \frac{\theta}{3} \log(x) \tag{8}$$

0.07 is the critical concentration for LaOCl:Eu^{3+} . A graph of $\log(\frac{I}{x})$ vs $\log(x)$ is drawn by determining the integrated intensity of $x = 0.07, 0.09$ that is a linear fit as in Fig. 8 Slope ($\frac{-\theta}{3}$) is obtained as -2.11 and thus θ is equal to 6.33. d-d interaction be held responsible for quenching of Europium ions in the host as θ value is close to 6. [23]

Commission International del'Eclairage (CIE) chromaticity diagram was used to estimate the accurate color of emission and its purity for the synthesized phosphor. Under an excitation of 395 nm, the chromaticity coordinates for $\text{La}_{1-x}\text{Eu}_x\text{OCl}$ ($x = 0.00, 0.01, 0.03, 0.05, 0.07, 0.09$) is (0.642, 0.358) indicating that the color emitted is in the red region as in Fig. 9 and results revealed that the LaOCl:Eu^{3+} phosphor is nearer to commercial red phosphors such as $\text{Y}_2\text{O}_3\text{:Eu}^{3+}$ (0.645, 0.347), $\text{Y}_2\text{O}_2\text{:S:Eu}^{3+}$ (0.647, 0.343) and National Television System Committee (NTSC) (0.67, 0.33) [24]. Table 3 gives the values of u', v', x, y, CCT , and color purity. Because the location of luminescent emission hardly varies, the CIE chromaticity coordinates of the phosphor

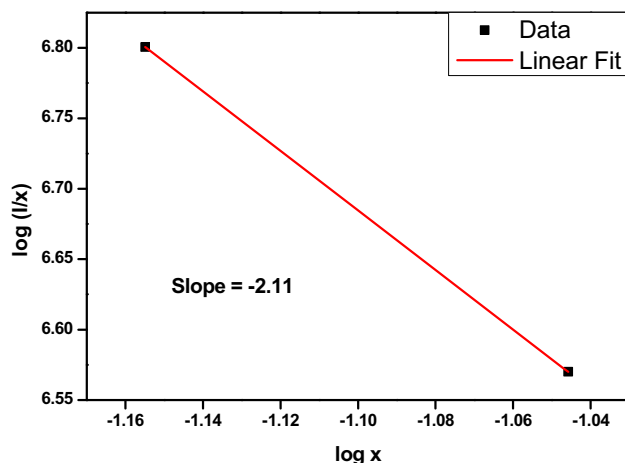


Fig. 8 The correlation between $\log(I/x)$ and $\log(x)$ of $\text{La}_{1-x}\text{Eu}_x\text{OCl}$ nanophosphors beyond quenching concentration

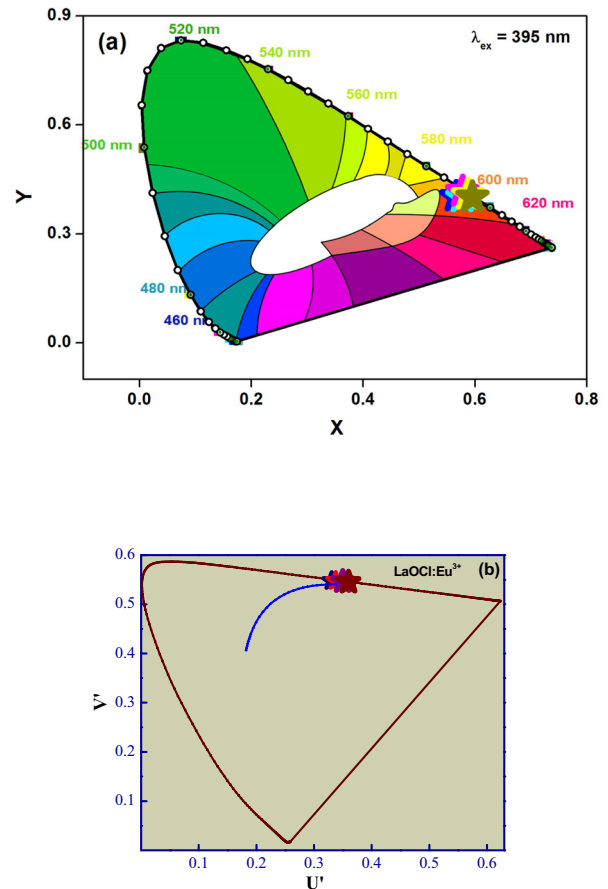


Fig. 9 a CIE. b CCT chromaticity diagram of $\text{La}_{1-x}\text{Eu}_x\text{OCl}$ ($0.00 \leq x \leq 0.09$) nanophosphors

were not dependent on the variation in europium concentration. Thus LaOCl:Eu^{3+} phosphor serve to be one among the constituent for the emission of white in relating it with phosphors emitting green-blue. The results reveal that LaOCl:Eu^{3+} phosphor serves to be a strong candidate for red phosphor materials.

3.6 Judd-Ofelt analysis

Judd-Ofelt theory [12, 13] favors in quantifying the impact of crystal field on Eu^{3+} ions spectral characteristics. JO parameters be useful in knowing the behavior of the covalency of Eu-O bonding and the local environment of the lanthanide ion. Also, Ω_2 intensity parameters (generally coupled with short-range coordination chemistry) and Ω_4 (that together with Ω_6 confine long-range effects) are beneficial to look into the structural environment and rigidity of inorganic matrix correspondingly [30, 31]. It is

figured out that their absolute values aren't utilized in knowing fundamental physics. Emission spectra were utilized to find JO intensity parameters.

The spontaneous emission probability of magnetic and electric dipole A^{md} and A^{ed} are respectively given by

$$A_{J'-J}^{md} = \frac{64\pi^4 \gamma^3 n^3 S_{md}}{3h(2J' + 1)} \quad (9)$$

$$A_{J'-J}^{ed} = \frac{64\pi^4 \gamma^3 e^2}{3h(2J' + 1)} \frac{n(n^2 + 2)^2}{9} \sum_{J=2,4} \Omega_J \langle {}^5D_0 | U^{(J)} | {}^7F_J \rangle^2 \quad (10)$$

here, n = refractive index of host, S_{md} = constant = 7.83×10^{-42} esu² cm² -the magnetic dipole line strength for Eu^{3+} is independent of host [32], γ = wavenumber, e = charge, $(2J' + 1)$ = the degeneracy of the initial state. The square reduced matrix elements $\langle {}^5D_0 | U^{(2)} | {}^7F_2 \rangle^2$ and $\langle {}^5D_0 | U^{(4)} | {}^7F_4 \rangle^2$ are 0.0032 and 0.0023 correspondingly.

The summation of the radiative transition probabilities is given by:

$$\sum_{J=0-4} A_{7F_J} = A_{ed\lambda} + A_{md\lambda} \quad (11)$$

Radiative lifetime τ_{rad} given by:

$$\tau_{rad} = \frac{1}{\sum_{J=0-4} A_{7F_J}} \quad (12)$$

The luminescence intensity of emission bands induced by the magnetic-dipole (I_{md}) and electric dipole (I_{ed}) transition is given by:

$$I_{ed} = \frac{hcA_{ed\lambda}N_J}{\lambda_{ed}}$$

And

$$I_{md} = \frac{hcA_{md\lambda}N_J}{\lambda_{md}} \quad (13)$$

where N_J gives a population of 5D_0 state of Europium.

The ratio of luminescence intensity of emission bands induced by the MD and ED transition is written as [33].

$$R = \frac{(n^2 + 2)^2 e^2 \lambda_{md}^4}{9n^2 S_{md} \lambda_{ed}^4} \Omega_{J=2,4} \langle {}^5D_0 | U^{(J)} | {}^7F_J \rangle^2 \quad (14)$$

Which can also be written as

$$R = \frac{\int I_{ed} d\lambda}{\int I_{md} d\lambda} \quad (15)$$

${}^5D_0 \rightarrow {}^7F_J$, $J = 1, 2, 4$, and 6 transitions of magnetic and electric dipole, respectively, $J = 3$ and 5 are forbidden whose square reduced matrix elements are zero as proposed by optical transition theory [33]. In Fig. 7b, transition due to $J = 6$ is unseen in emission spectrum of LaOCl:Eu^{3+} nanophosphors. Ω_2 and Ω_4 may be estimated by relating Eqs. (14) and (15).

Emission from an excited to its lower levels-The branching ratio β is written as [34]:

$$\beta = \frac{A_{ed\lambda,md\lambda}}{\sum_{J=0-4} A_{7F_J}} \quad (16)$$

The JO intensity parameters, transition probabilities, branching ratios, radiative lifetime, and asymmetric ratios for $\text{La}_{1-x}\text{Eu}_x\text{OCl}$ are tabulated in Table 2. All molar concentrations exhibited a trend $\Omega_2 > \Omega_4$ JO parameters indicating that Eu^{3+} ion occupies asymmetric sites [34]. Higher value of Ω_2 was obtained for $x = 0.07$ in comparison to other concentrations representing that at this concentration the effect of the crystal field of LaOCl is high upon Eu^{3+} ions giving rise to forced ED transition ${}^5D_0 \rightarrow {}^7F_2$ being highly intense than the ${}^5D_0 \rightarrow {}^7F_1$ -MD transition (is obvious in the PL). The Eu^{3+} ions lack inversion symmetry considerably as specified by asymmetric ratio values as well. Thus one can conclude, Eu^{3+} ions favor non-centrosymmetric sites in the host, thus ensuing in a weaker ${}^5D_0 \rightarrow {}^7F_1$ transition and a strong ${}^5D_0 \rightarrow {}^7F_2$ transition. The radiative lifetime of every molar concentration is evaluated and is obtained to be ~ 1.56 ms for the optimized concentration. This result indicates the aptness of LaOCl:Eu^{3+} nanophosphor as red emission and an effectual material for luminescence.

3.7 Electrical and dielectric properties.

Conductivity measurements were carried out with frequency from 10 Hz to 8 MHz at room temperature. The AC conductivity of $\text{La}_{1-x}\text{Eu}_x\text{OCl}$ ($0.01 \leq x \leq 0.09$) are evaluated using the following equation:

$$\sigma_{AC} = 2\pi f \epsilon' \epsilon_0 \tan \delta \quad (17)$$

Here ϵ' = real part of dielectric constant, f = applied AC signal frequency, ϵ_0 = permittivity of free space and $\tan \delta$ = tangent loss.

Table 2 Calculated values of JO parameters for La_{1-x}Eu_xOCl phosphor

λ_{ex} (nm)	Eu ³⁺ conc x	Judd–Ofelt intensity parameters (10 ⁻²⁰ cm ²)		Transitions	A_{0-J} (J=1,2,4) (s ⁻¹)	A_{7F_1} (s ⁻¹)	τ_{rad} (ms)	(%)	Asymmetry ratio
		Ω_2	Ω_4						
395	0.01	5.98	3.13	⁵ D ₀ → ⁷ F ₁	79.81	570.34	1.75	68.46	4.72
				⁵ D ₀ → ⁷ F ₂	390.43				
				⁵ D ₀ → ⁷ F ₄	100.1				
	0.03	6.36	3.22	⁵ D ₀ → ⁷ F ₁	79.81	607.98	1.64	69.40	5.10
				⁵ D ₀ → ⁷ F ₂	421.96				
				⁵ D ₀ → ⁷ F ₄	106.21				
	0.05	6.42	3.30	⁵ D ₀ → ⁷ F ₁	79.81	601.28	1.66	69.70	5.36
				⁵ D ₀ → ⁷ F ₂	419.05				
				⁵ D ₀ → ⁷ F ₄	102.42				
	0.07	6.97	3.40	⁵ D ₀ → ⁷ F ₁	79.81	640.65	1.56	71.04	5.49
				⁵ D ₀ → ⁷ F ₂	455.14				
				⁵ D ₀ → ⁷ F ₄	105.70				
	0.09	6.74	3.39	⁵ D ₀ → ⁷ F ₁	79.81	628.01	1.59	70.02	5.31
				⁵ D ₀ → ⁷ F ₂	439.74				
				⁵ D ₀ → ⁷ F ₄	108.46				

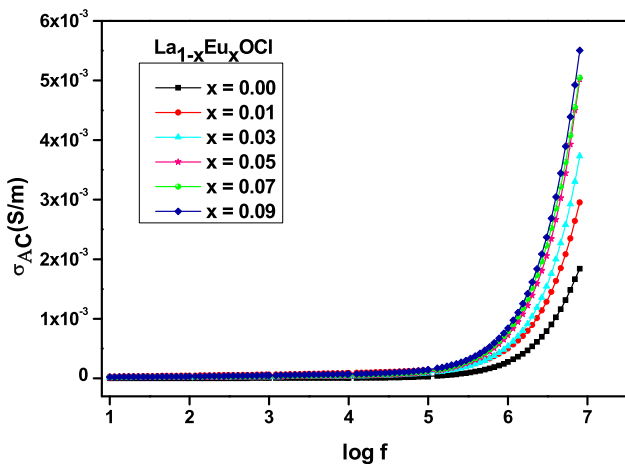


Fig. 10 Variation of AC conductivity with frequency of La_{1-x}Eu_xOCl (0.01 ≤ x ≤ 0.09) nanophosphors

Conducting property of materials relies on frequency which is due to the conduction between the localized states [35]. Figure 10 indicates the frequency dependence of conductivity for La_{1-x}Eu_xOCl (0.01 ≤ x ≤ 0.09). In the range of frequency 10 Hz to 8 MHz, the conductivity of La_{1-x}Eu_xOCl (0.01 ≤ x ≤ 0.09) displays two distinct regions, a plateau, and

dispersion. The conductivity is frequency independent (dc conductivity) in the plateau region due to long-range movement of charge carriers [36]. In the higher frequency range (dispersion) with increasing frequency, the conductivity which is AC tracks an exponential power law revealing a rise [37]. AC conductivity is due to the consequence of more amounts of trapped charge carriers which doesn't contribute to long-range dc conduction process resulting in more ac conductivity towards higher frequency range [38, 39].

The property of the dielectric material is inferred through the behavior of the material in a parallel plate capacitor. The capacitance of the capacitor in free space separated with a distance 't' may be written as:

$$C_o = \frac{\epsilon_0 A}{t} \tag{18}$$

where, ϵ_0 = permittivity (free space), t = distance between the plates, A = area of the plate.

The capacitance of a capacitor with a dielectric medium between the plates is as follows:

$$C_m = \frac{\epsilon_m A}{t} \tag{19}$$

Table 3 CIE color coordinates and CCT values for $\text{La}_{1-x}\text{Eu}_x\text{OCl}$ ($0.00 \leq x \leq 0.09$) Nano phosphor

λ_{ex} (nm)	Concentration of Eu^{3+} x	x	y	u'	v'
395	0.01	0.640	0.360	0.428	0.5534
	0.03	0.635	0.361	0.427	0.5537
	0.05	0.639	0.359	0.425	0.5537
	0.07	0.642	0.358	0.427	0.536
	0.09	0.640	0.353	0.429	0.5533

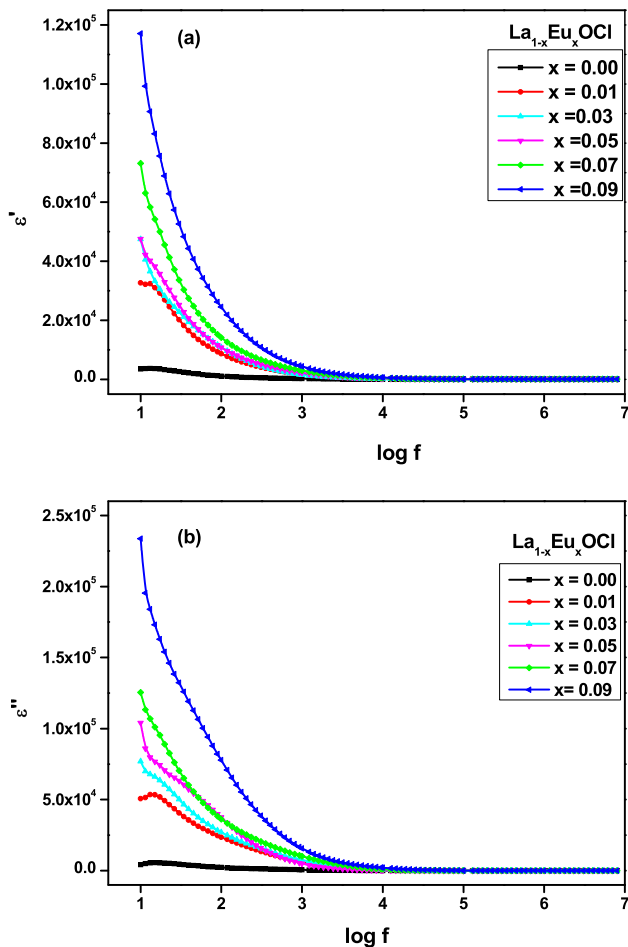


Fig. 11 Variation of dielectric constant as a function of frequency (a) real part of dielectric constant (b) imaginary part of dielectric constant of $\text{La}_{1-x}\text{Eu}_x\text{OCl}$ ($0.01 \leq x \leq 0.09$) nanophosphors

here ϵ_m = permittivity of the medium.

The ratio between C_m and C_0 gives the dielectric constant denoted by ' ϵ ' also called the relative permittivity of the medium (ϵ_r)

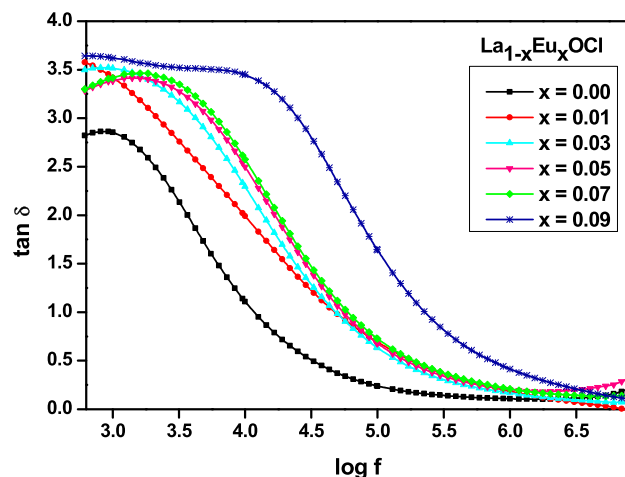


Fig. 12 Frequency dependence of dielectric loss of $\text{La}_{1-x}\text{Eu}_x\text{OCl}$ ($0.01 \leq x \leq 0.09$) nanophosphors

$$\frac{C_m}{C_0} = \frac{\epsilon_m}{\epsilon_0} \quad (20)$$

The dielectric constant in complex form is given by:

$$\epsilon^* = \epsilon' - j\epsilon'' \quad (21)$$

where ϵ' & ϵ'' are real (relative permittivity) and imaginary part of dielectric constant respectively and ϵ^* is also written as [40]

$$\epsilon^* = \frac{1}{j\omega C_0 Z^*} \quad (22)$$

ω = angular frequency, C_0 = free space capacitance.

$$\tan \delta = \frac{\epsilon'}{\epsilon''} = \frac{M'}{M''} \quad (23)$$

The variation of dielectric constant (ϵ' and ϵ'') with frequency of $\text{La}_{1-x}\text{Eu}_x\text{OCl}$ ($0.01 \leq x \leq 0.09$) phosphor is shown in Fig. 11a and b and it is clear that ϵ' declines as frequency increases and reaches constant indicating after a specific frequency, hopping of electron may not go along the alternating field [41].

Because mobility of electrons is more than holes, the influence of holes in the process of polarization is least and decreases considerably at low frequencies, and hence the overall polarization and dielectric constant reduce. The types of polarization held responsible for variation of dielectric constant of material are ionic, electronic, orientation, and space charge polarization. Interfacial polarization led to a decrease in ϵ' and being constant at higher frequencies for the present phosphor.

Equation (23) represents the dielectric loss ' $\tan \delta'$ ', a phase shift related to a time lag between an applied and induced voltage leads to energy dissipation and loss currents in AC circuits which require no charge carrier migration. A graph of tangent loss vs $\log f$ of $\text{La}_{1-x}\text{Eu}_x\text{OCl}$ ($0.01 \leq x \leq 0.09$) phosphor is shown in Fig. 12 which reveals a peaking behavior due to resonance matching [42]. Because of the energy exchange to oscillating ions from the applied field, no power loss is observed within the investigated frequency range.

Materials with lesser values of dielectric loss are best suited for high-frequency applications like microwave devices and the present phosphor $\text{La}_{1-x}\text{Eu}_x\text{OCl}$ ($0.01 \leq x \leq 0.09$) have exhibited much lower values of dielectric loss [43, 44].

4 Conclusions

A series of red light-emitting LaOCl phosphor with different mole concentrations of europium as dopant $\text{La}_{1-x}\text{Eu}_x\text{OCl}$ ($0 \leq x \leq 0.09$) was synthesized by taking stoichiometric amount of La_2O_3 , Eu_2O_3 , and NH_4Cl (excess 20%) via solid-state method which exhibited a tetragonal structure with space group $P4/nmm$ (No. 129). Morphological investigations are made by SEM and TEM exhibiting the agglomeration form of the phosphor. The size of the particle is in the range of 32 nm. From the excitation spectra, it is noted that $\text{La}_{1-x}\text{Eu}_x\text{OCl}$ can be proficiently excited using near UV, UV blue, UV, and hence is suitable for present-day solid-state applications. Concerning the transition ${}^5\text{D}_0 \rightarrow {}^7\text{F}_2$ for $x = 0.07$, the phosphor exhibited the highest luminescence intensity at 617 nm. The CIE color coordinates were found as (x , $y = 0.642, 0.358$) which is nearer to the commercial Phosphor. The value of R_c between Eu ions in the host is found to be 9.28 indicating multipole-multipole interactions probable cause for quenching

(further than $x = 0.07$ doping Eu^{3+}). From JO analysis regardless of Eu^{3+} concentration, $\Omega_2 > \Omega_4$ representing asymmetric environment around the activator. Asymmetric ratio values being higher propose a dwelling of Eu^{3+} ion in sites without an inversion center with low symmetry. It is observed at the lower frequency the nanophosphor displays a greater magnitude of dielectric constant and loss that declined significantly as frequency increases. For $\text{La}_{1-x}\text{Eu}_x\text{OCl}$ ($0.01 \leq x \leq 0.09$) at a higher frequency, lower values of $\tan \delta$ marks its appropriateness for high-frequency microwave device applications moreover because of more stability, effective PL intensity, best CIE chromaticity these phosphors are potentially used in display devices.

References

1. N. Dhananjaya, S.R. Yashodha, C. Shivakumara, Synthesis, characterization and spectroscopic properties of $\text{GdOF}:\text{Eu}^{3+}$ phosphors and their Judd–Ofelt analysis. *Int. J. Nanotechnol.* **14**, 727–738 (2017). <https://doi.org/10.1504/IJNT.2017.086759>
2. G. Blasse, A. Bril, Fluorescence of Eu^{3+} -activated lanthanide oxyhalides LnOX . *J. Chem. Phys.* **46**, 2579–2582 (1967). <https://doi.org/10.1063/1.1841086>
3. U. Rambabu, A. Mathur, S. Buddhudu, Fluorescence spectra of Eu^{3+} and Tb^{3+} -doped lanthanide oxychloride powder phosphors. *Mater. Chem. Phys.* **61**, 156–162 (1999). [https://doi.org/10.1016/S0254-0584\(99\)00122-4](https://doi.org/10.1016/S0254-0584(99)00122-4)
4. U. Rambabu, N.R. Muniratham, T.L. Prakash, S. Buddhudu, Emission spectra of $\text{LnPO}_4:\text{RE}^{3+}$ ($\text{Ln} = \text{La, Gd}$; $\text{RE} = \text{Eu, Tb}$ and Ce) powder phosphors. *Mater. Chem. Phys.* **78**, 160–169 (2002). [https://doi.org/10.1016/S0254-0584\(02\)00294-8](https://doi.org/10.1016/S0254-0584(02)00294-8)
5. V.V. Bunda, M.V. Shtilikha, V.M. Goldvei, Thermal stability of lanthanide oxide chlorides. *Russ. J. Inorg. Chem.* **29**, 1741 (1984)
6. E. Antic-Fidancev, J. Holsa, M.L. Blaise, P. Porcher, Observation and simulation of the energy-level scheme of the Pr^{3+} ion in REOCl . *J. Chem. Soc.: Faraday Trans* **87**, 3625–3630 (1991). <https://doi.org/10.1039/FT9918703625>
7. G. Li, T. Long, Y. Song, G. Gao, J. Xu, B. An, S. Gan, G. Hong, Preparation and luminescent properties of $\text{CaAl}_2\text{O}_4:\text{Eu}^{3+}$, R^{2+} ($\text{R} = \text{Li, Na, K}$) phosphors. *J. Rare Earths* **28**, 22–25 (2010). [https://doi.org/10.1016/S1002-0721\(09\)60042-9](https://doi.org/10.1016/S1002-0721(09)60042-9)
8. Y. Guo, X. Yu, J. Liu, X. Yan, Photoluminescence of Eu^{2+} -activated $\text{Na}_{1-x}\text{Al}_{1-x}\text{Si}_{1+x}\text{O}_4$ upon UV excitation. *J. Rare*

- Earths **28**, 34–36 (2010). [https://doi.org/10.1016/S1002-0721\(09\)60045-4](https://doi.org/10.1016/S1002-0721(09)60045-4)
9. K. Rajeswar, N.R. Tacconi, C.R. Chenthamarakshan, Semiconductor-based composite materials: Preparation, properties and performance. *Chem. Mater* **13**, 2765–2782 (2001). <http://doi.org/10.1021/cm010254z>
 10. A.P. Alivisatos, Semiconductor clusters, nanocrystals and quantum dots. *Science* **271**, 933–937 (1996). DOI:<https://doi.org/10.1126/science.271.5251.933>
 11. M.A. Anderson, S. Gorer, R.M. Penner, A hybrid electrochemical/chemical synthesis of supported, luminescent cadmium sulfide nanocrystals. *J. Phys. Chem. B* **101**, 5895–5899 (1997). <https://doi.org/10.1021/jp970627c>
 12. A. Choubey, S. Som, M. Biswas, S.K. Sharma, Characterization of optical transitions of Eu^{3+} in lanthanum oxychloride nanophosphor. *J. rare earths* **29**, 345–348 (2011). [https://doi.org/10.1016/S1002-0721\(10\)60457-7](https://doi.org/10.1016/S1002-0721(10)60457-7)
 13. B.R. Judd, B R, Optical absorption intensities of rare-earth ions. *Phys. Rev.* **127**, 750–761 (1962). <https://doi.org/10.1103/PhysRev.127.750>
 14. G.S. Ofelt, Intensities of crystal spectra of rare-earth ions. *J. Chem. Phys.* **37**, 511–520 (1962). <https://doi.org/10.1063/1.1701366>
 15. M.T. Rahman, M. Vargas, C.V. Ramana, Structural characteristics, electrical conduction and dielectric properties of gadolinium substituted cobalt ferrite. *J. Alloys Compd.* **617**, 547–562 (2014). <https://doi.org/10.1016/j.jallcom.2014.07.182>
 16. S.W. Kim, K. Jyoko, T. Masui, N. Imanaka, Green-emitting (La,M,Tb)OCl (M = Mg, Ca, and Sr) phosphors. *Opt. Mater.* **35**, 280–284 (2012). <https://doi.org/10.1016/j.optmat.2012.08.022>
 17. S. Park, S.H. Cho, Spectral-converting study of $\text{La}_{1-m-n}\text{Er}_m\text{Yb}_n\text{OCl}$ ($m = 0.001-0.2$, $n = 00.1$) phosphors. *J. Lumin.*, **153**, 90–95 (2014). <https://doi.org/10.1016/j.jlumin.2014.03.023>
 18. Z.X. Wei, Y. Wang, X.J. Zhang, C.W. Hu, Combustion synthesis and effect of LaMnO_3 and LaOCl powder mixture on HMX thermal decomposition. *Thermochim. Acta* **499**, 111–116 (2010). <https://doi.org/10.1016/j.tca.2009.11.010>
 19. A.K. Zak, W.H.A. Majid, M. Darroudi, Facile synthesis and characterization of lanthanum (III) oxychloride nanoparticles using a natural polymeric matrix. *Mater. Chem. Phys.* **136**, 705–709 (2012). <https://doi.org/10.1016/j.matchemphys.2012.07.045>
 20. S.S. Lee, H.I. Park, C.H. Joh, S.H. Byeon, Morphology dependent photoluminescence property of red-emitting $\text{LnOCl}:\text{Eu}^{3+}$ (Ln = La and Gd). *J. Solid State Chem* **180**, 3529–3534 (2007). <https://doi.org/10.1016/j.jssc.2007.10.020>
 21. J. Lee, Q. Zhang, F. Saito, Mechanochemical synthesis of LaOX (X = Cl, Br) and their solid -state solutions. *J. Solid State Chem.* **160**, 469–473 (2001). <https://doi.org/10.1006/jssc.2001.9276>
 22. S.G. Prasanna Kumar, R. Hari Krishna, Nagaraju Kottama, P. Krishna Murthy, C. Manjunatha, R. Preetham, C. Shivakumara, T. Thomas, **Understanding the photoluminescence behaviour in nano $\text{CaZrO}_3:\text{Eu}^{3+}$ pigments by Judd-Ofelt intensity parameters**, *Dyes and Pigments*, **150**, 306–314 (2018). <https://doi.org/10.1016/j.dyepig.2017.12.022>
 23. S.R. Yashodha, N. Dhananjaya, C. Manjunath, Synthesis and photoluminescence properties of Sm^{3+} doped LaOCl phosphor with reddish-orange emission and its Judd-Ofelt analysis. *Mater. Res. Express* **7**, 15003–15019 (2020). <https://doi.org/10.1088/2053-1591/ab57a6>
 24. A. Khorsand Zak, W.H. Abd, M. Darroudi, synthesis and characterization of lanthanum (III) oxychloride nanoparticles using a natural polymeric matrix. *Mater Chem Phys.* **136**, 705–709 (2012). <https://doi.org/10.1016/j.matchemphys.2012.07.045>
 25. S.R. Yashodha, N. Dhananjaya, C. Shivakumara, Study of (La, Gd)OCl: Eu^{3+} phosphors for WLEDs application: photoluminescence and Judd-Ofelt analysis. *Int. J. Nanotechnol.* **14**, 801–815 (2017). <https://doi.org/10.1504/IJNT.2017.086765>
 26. J.K. Park, S.M. Park, C.H. Kim, H.D. Park, S. Choi, Photoluminescence properties of the Eu^{3+} in La_2O_3 . *J. Mater. Sci. Lett.* **20**, 2231–2232 (2001). <https://doi.org/10.1023/A:1017997320503>
 27. C. Manjunath, M.S. Rudresha, B.M. Walsh, R. Hari Krishna, B.S. Panigrahi, B.M. Nagabhushana, Optical absorption intensity analysis using Judd-Ofelt theory and photoluminescence investigation of orange-red $\text{Sr}_2\text{SiO}_4:\text{Sm}^{3+}$ nanopigments. *Dyes and Pigments.* **148**, 118–129 (2018). <https://doi.org/10.1016/j.dyepig.2017.08.036>
 28. G. Blasse, Energy transfer in oxidic phosphors. *Phys Lett* **28**, 444–445 (1968). [10.1016/0375-9601\(68\)90486-6](https://doi.org/10.1016/0375-9601(68)90486-6)
 29. N. Dhananjaya, C. Shivakumara, R. Saraf, S. Behera, H. Nagabhushana, Comparative study of Eu^{3+} -activated LnOCl (Ln = La and Gd) phosphors and their Judd-Ofelt analysis. *J. Rare Earths* **33**, 946–953 (2015). [https://doi.org/10.1016/S1002-0721\(14\)60510-X](https://doi.org/10.1016/S1002-0721(14)60510-X)
 30. L.G. Van Uitert, Characterization of energy transfer interactions between rare earth ions. *J Electrochem Soc.* **114**, 1048–1053 (1967). <https://doi.org/10.1149/1.2424184>
 31. K. Christian, R. Jorgensen, Judd-Ofelt parameters and chemical bonding. *J Less Common Met* **93**, 107–112 (1983). [https://doi.org/10.1016/0022-5088\(83\)90454-X](https://doi.org/10.1016/0022-5088(83)90454-X)

32. F.K. William, Optical absorption and fluorescence intensities in several rare-earth-doped Y₂O₃ and LaF₃ single crystals. *Phys Rev* **145**, 325–337 (1966). <https://doi.org/10.1103/PhysRev.145.325>
33. R. Venkatesh, N. Dhananjaya, M.K. Sateesh, J.P. Shabaa Begum, S.R. Yashodha, H. Nagabhushana, C. Shivakumara, Effect of Li, Na, K cations on photoluminescence of GdAlO₃:Eu³⁺ nanophosphor and study of Li cation on its antimicrobial activity. *J. Alloys Compd.* **732**, 725–739 (2018). <https://doi.org/10.1016/j.jallcom.2017.10.117>
34. X. Wang, C. Liu, T. Yuaand, X. Yan, Controlled synthesis, photoluminescence and the quantum cutting mechanism of Eu³⁺ doped NaYbF₄ nanotubes. *Phys. Chem. Chem. Phys.* **16**, 13440–13446 (2014). <https://doi.org/10.1039/C4CP01263A>
35. Y. Tian, B. Chen, R. Hua, J. Sun, L. Cheng, H. Zhong, X. Li, J. Zhang, Y. Zheng, T. Yu, L. Huangand, H. Yu, Optical transition, electron-phonon coupling and fluorescent quenching of La₂(MoO₄)₃:Eu³⁺ phosphor. *J. Appl. Phys.* **109**, 053511–053516 (2011). <https://doi.org/10.1063/1.3551584>
36. F. Liu, Y. Fang, N. Zhang, J. Hou, Z. Ma, G. Zhao, Blue light excited Li₆CaLa₂M₂O₁₂:Eu³⁺ (M = Ta, Sb) red emitting phosphors: structure and Photoluminescence properties. *Ceram. Int.* **40**, 14781–14786 (2014). <https://doi.org/10.1016/j.ceramint.2014.06.069>
37. G. Yellaiah, M. Nagabhushanam, Variable range hopping (VRH) conductivity, ac conductivity and dielectric studies on Sm³⁺ doped Cd_{0.8}Zn_{0.2}S semiconductor compounds. *Journal of Crystal Growth.* **421**, 33–38 (2015). <https://doi.org/10.1016/j.jcrysgro.2015.04.006>
38. C.R. Mariappan, G. Govindaraj, S.V. Rathan, G.V. Prakash, Preparation, characterization, ac conductivity and permittivity studies on vitreous M₄AlCdP₃O₁₂ (M = Li, Na, K) system. *Mater Sci Eng.* **121**, 2–8 (2005). <https://doi.org/10.1016/j.mseb.2004.11.005>
39. A.K. Jonscher, *Universal Relaxation Law* Chelsea Dielectric Group, London. (1996) (Chap. 5)
40. J. Hazarikaand, A. Kumar, Enhanced ac conductivity and dielectric relaxation properties of polypyrrole nanoparticles irradiated with Ni¹²⁺ swift heavy ions. *Nuc. Inst. Meth. Phys. Res. B.* **333**, 73–79 (2014). <https://doi.org/10.1016/j.nimb.2014.04.019>
41. M.K. Anupama, B. Rudraswamy, N. Dhananjaya, Investigation on impedance response and dielectric relaxation of Ni-Zn ferrites prepared by self-combustion technique. *J. Alloys Compd.* **706**, 554–561 (2017). <https://doi.org/10.1016/j.jallcom.2017.02.241>
42. G.P. Johari, K. Pathmanathan, The dipolar and conductivity relaxations in ionic conductors. *Phys. Chem. Glasses* **29**, 219–224 (1988).
43. M. Hashim, S. Kumar, S.E. Shirsath, E.M. Mohammed, H. Chung, R. Kumar, Studies on the activation energy from the ac conductivity measurements of rubber ferrite composites containing manganese zinc ferrite. *Phy. B: Condens. Matter* **407**, 4097–4103 (2012). <https://doi.org/10.1016/j.physb.2012.06.006>
44. A. Azam, Microwave assisted synthesis and characterization of Co-doped Cu ferrite nanoparticles. *J. Alloys Compd.* **540**, 145–153 (2012). <https://doi.org/10.1016/j.jallcom.2012.06.068>

Publisher's Note Springer Nature remains neutral with regard to jurisdictional claims in published maps and institutional affiliations.